

Fluctuating growth rates link turnover and unevenness in species-rich communities

Emil Mallmin^{1,*}, Arne Traulsen¹, and Silvia De Monte^{1,2}

¹Max Planck Institute for Evolutionary Biology, Plön, Germany

²Institut de Biologie de l'ENS (IBENS), Département de Biologie, Ecole Normale Supérieure, CNRS, INSERM, Université PSL, 75005 Paris, France

*mallmin@evolbio.mpg.de

Wednesday 11th June, 2025

The maintenance of diversity, the ‘commonness of rarity’, and compositional turnover are ubiquitous features of species-rich communities. Through a stylized model, we consider how these features reflect the interplay between environmental stochasticity, intra- and interspecific competition, and dispersal. We show that, even when species have the same time-average fitness, fitness fluctuations tend to drive the community towards ever-growing unevenness and species extinctions, but self-limitation and/or dispersal allow high-diversity states to be sustained. We then analyze the species-abundance distribution and the abundance distribution of individual species over time in such high-diversity states. Their shapes vary predictably along two axes—Exclusion-Stabilization and Exclusion-Buffering—that describe the relative strength of the underlying ecological processes. Predicted shapes cover different empirically observed cases, notably power-law and unimodal distributions. An effective focal-species model allows us to relate static abundance distributions with turnover dynamics, also when species have different mean fitness. The model suggests how community statistics and time series of individual species can inform on the relative importance of the ecological processes that structure diversity.

Species-rich communities—for instance tropical forests, birds, plankton and microbiomes—pose a series of fundamental questions. In light of the competitive exclusion principle [1–3], it is counterintuitive that so many species coexist in environments that, seemingly, offer few axes of niche differentiation. At the same time, coexistence is not equitable: at any given time and place of sampling, the vast majority of species have low abundance in comparison to a few highly abundant species [4, 5]. Some communities, notably tropical trees [6, 7], even display hyperdominance, where a few species account for the majority of all individuals. Species abundance distributions (SADs) quantify the spectrum from dominance to rarity in a community, and tend to display only a few qualitative shapes depending on the scale and intensity of sampling, with long-lasting debates about the best-fitting quantitative form [4, 8–11]. Yet underlying the relative regularity of SADs is high variability in any given species’ abundance across local samples. What factors—systematic or random—determine when and where a species is locally dominant or rare? Species’ environmental tolerance ranges and the makeup of regional species pools set constraints, but most of the variation in local community composition remains unexplained by readily measured environmental factors [12, 13]. Aggregating species into functional groups, or focussing on regionally common species increases predictability and regularity, but individual species tend to fluctuate in abundance for reasons that are not well understood [14, 15].

The stylized facts of species-rich coexistence, the ‘commonness of rarity’, and pervasive species turnover originate in different ecological mechanisms in taxonomically and environmentally distant communities. The reality of an ocean-drifting phytoplankter, extracting what amount of

light and nutrients it can before being eaten by a zooplankter, is very different from the tropical tree seedling growing to fill the gap in the canopy opened by a full-grown rival struck down by lightning [16]. Nonetheless, competition, dispersal, and demographic and environmental forms of stochasticity are general processes that shape all species-rich communities to varying extents [17, 18]. The ubiquity of the aforementioned biodiversity patterns suggests that an explanation is rightly sought in terms of the interactions of a few such high-level processes. Mathematical models of community dynamics allow to explore the non-trivial emergence of patterns from processes.

Neutral theories [19–22] explain how realistic species abundance distributions can emerge from a balance of neutral drift to extinction (i.e. through unbiased randomness of birth and death events) and re-immigration into the local patch from the regional species pool. Metacommunities exhibiting a spatiotemporal buffering effect offer a consistent view on how regional species pools can remain diverse on long timescales through sufficient dispersal between many local patches [23–25]. However, demographic stochasticity alone is inconsistent with the statistics and timescales of empirical abundance fluctuations [26–28]. Time-averaged neutral theory (TAN) [29, 30] addresses this fundamental issue by incorporating environmental stochasticity, appearing as species-specific fluctuations in fitness, to represent unmodelled variability in resources, abiotic conditions, predator pressure, etc. While species differ in their fitnesses at any given time, all species are assumed to have comparable fitnesses averaged over a sufficiently long time.

At the other end of a ‘niche–neutral continuum’ [31–33], deterministic models of heterogeneous competition (generalized Lotka-Volterra [34, 35] and consumer-resource

models [36, 37]) show that under quite generic assumptions, species-rich and stable coexistence equilibria require species to be weakly (or sparsely) coupled with one another; in other words, to have small niche overlap, whereas neutral theories assume a large overlap [38]. A stable equilibrium ignoring fluctuations may be an appropriate description of some species-rich communities on shorter timescales. Nonetheless, the species abundance distributions predicted from weak and heterogeneous competition are unrealistically *even*, unless special assumptions on the distributions of model parameters such as carrying capacities (e.g. a power law) are posited [39]. Interestingly, it has been widely reported that the regime of strong interactions, rather than implying pervasive competitive exclusion, can drive a local turnover of many rare and few abundant species if immigration is present [40–44]. Such turnover reflects deterministic chaos due to nonlinear interactions, but the time series of a focal species largely resembles logistic growth under environmental noise [43, 45], forging a phenomenological link to the time-averaged neutral models.

A pressing challenge for theoretical ecology is to synthesize the results from an array of partially overlapping models—neutral or niche-based, stochastic or deterministic, well-mixed or spatially structured—towards a mathematically robust understanding of species-rich community patterns. To this end, we consider here a model incorporating strong but competitively neutral interactions and time-averaged neutral environmental stochasticity within a Lotka-Volterra framework [46–49]. Recently, van Nes et al [48] employed such a model to suggest an explanation for the (hyper-)dominance of species in a wide range of community data sets. They draw attention to the ‘stickiness’ effect (called ‘diffusive trapping’ in prior work by Dean and Shnerb [50]), whereby the scaling of abundance fluctuations biases species that become rare to remain rare. We present a detailed mathematical exposition of this phenomenon, through an exact mapping to replicator dynamics and to condensation phase transitions in physics, and explain why noise in fact drives the community toward unevenness, and eventually monodominance, even in very large communities. We show that buffering or stabilizing mechanisms are necessary for the maintenance of diversity, such as immigration (as in parallel work by Kessler and Shnerb [49]) or sufficiently strong intraspecific competition. We then characterize the SAD of the community, whose shape interpolates between a few empirically relevant archetypes, including power law and log-normal-like. We find that these different shapes can be classified by only two parameters that quantify the relative importance of environmental noise, buffering, and stabilizing processes. We use an approximate single-species model to relate the shape of the SAD to the fluctuation statistics of individual species. Finally, we consider heterogeneity in single-species time-averaged fitness, and discuss how the model can bridge community-level patterns and the dynamics of individual species.

MODEL

Community dynamics

We consider a pool of S species that in a local community of interest have abundances $n_i(t)$ ($i = 1, 2, \dots, S$) at time t . The intrinsic fitness of a species i is defined by its per capita growth rate $r_i(t)$ in the absence of within-community interactions, which fluctuates in time in response to a variable environment. Following classical hypotheses, we take interactions to be dominated by competition, such that any pair of individuals compete with identical strength μ (i.e. *neutral competition*), except that conspecifics experience an additional self-limitation of strength ε , due to higher niche overlap. Additionally, we consider a small, constant rate of net immigration λ , intended as a simplified representation of a metacommunity structure. Denoting the total abundance by $N(t) = \sum_{j=1}^S n_j(t)$, these assumptions translate into the growth equation:

$$\dot{n}_i(t) = n_i(t)[r_i(t) - \mu N(t) - \varepsilon n_i(t)] + \lambda. \quad (1)$$

We will also consider an explicit metacommunity structure by replacing λ with

$$\sum_{\beta=1}^M (d_{\alpha\beta} n_{i,\beta}(t) - d_{\beta\alpha} n_{i,\alpha}(t)), \quad (2)$$

where $n_{i,\alpha}(t)$ is the abundance of species i in patch α , and $d_{\alpha\beta}$ a species-independent dispersal rate from patch β to α .

While the community dynamics encompasses some of the most broadly relevant processes, there are also notable omissions. We do not include demographic stochasticity, arising from the discrete nature of individual birth and deaths. To nonetheless allow for the extinction of rare species we introduce a threshold n_{ext} below which abundances are set to zero. Furthermore, species coexistence through the storage effect (i.a. noise-induced stabilization) [51, 52] has been precluded, since the fluctuating fitnesses and competition appear additively in the growth rate. For perspectives on these effects in species-rich communities, we refer to several recent works [30, 49, 53].

Fluctuating fitnesses

The fluctuating fitnesses $r_i(t)$ represent the net effect of a complex and time-varying environment that we do not model explicitly, and could include effects of interactions outwith the community (e.g. grazing, predation), varying resource availabilities, abiotic environment (e.g. temperature, salinity), and so on. For simplicity, we assume the $r_i(t)$ ’s to be statistically independent between species, and independent of the abundance of any species, thereby asserting that the important density-dependent mechanisms in the community are in the main captured by the explicit competition terms in Eq. (1). We characterize the fitness statistics by the expected value r_i^* , the variance σ_r^2 , and the autocorrelation time τ . Unless otherwise indicated, we will assume species are time-average neutral, meaning $r_i^* = r^*$

[29]. Fitness variance and autocorrelation will be species-independent throughout.

As a concrete model of fluctuations we choose an Ornstein-Uhlenbeck process

$$\tau \dot{r}_i(t) = -(r_i(t) - r_i^*) + \sqrt{\gamma} \dot{W}_i(t). \quad (3)$$

Here, $\gamma := 2\sigma_r^2\tau$, and $\dot{W}_i(t)$ is a white noise (formally defined by its integral being a Wiener process). At stationarity, the fitness is $\mathcal{N}(r_i^*, \sigma_r)$ -distributed and the autocorrelation function decays exponentially with rate $1/\tau$. Taking in this way $r_i(t)$ to be a coloured noise has several conceptual advantages over supposing it is a white noise according to $r_i(t) = r_i^* + \omega \dot{W}_i$: we do not implicitly assume environmental fluctuation timescales are fast (perhaps reasonable for elephants, but less so for *E. coli*); the parameters σ_r, τ have a clearer biological interpretation than the noise amplitude ω ; and we can ignore subtleties of stochastic calculus convention. The white noise model for $r_i(t)$ can be recovered from Eq. (3) in the limit $\tau \rightarrow 0, \sigma_r \rightarrow \infty$, while keeping $\omega^2 = 2\sigma_r^2\tau$ constant, implying the Stratonovich stochastic calculus [54].

The numerical implementation of the model is described in [Appendix B](#).

RESULTS

Randomly fluctuating fitnesses drive diversity loss

To establish a baseline for the effect of fitness fluctuations on species coexistence and diversity, consider the special case of Eq. (1) with neutral competition ($\varepsilon = 0$) and no immigration ($\lambda = 0$):

$$\dot{n}_i(t) = n_i(t)[r_i(t) - \mu N(t)]. \quad (4)$$

In the headings below, we study the dynamics of this system, first in simulation and then analytically. We provide first a summary of the main conclusions.

Coexistence in Eq. (4) is only transient: communities progress toward pronounced unevenness, and eventually monodominance. This is true even in the absence of an extinction cutoff, in which case it takes progressively longer for the identity of the dominant species to change. The stickiness effect forms part of the explanation [30, 48]: Because the magnitude of abundance fluctuations is proportional to the current abundance, the rarer a species becomes, the larger (and hence more infrequent) the fitness fluctuation needed to escape rarity. The other part can be traced to the growing variance of fitnesses integrated over time, despite the convergence of time-averaged fitnesses toward r^* .

A key measure of the effectiveness of stochastic exclusion is the time t_c it takes for an initially even community to become composed of a few dominant species. We show that it scales as $\ln(S)/\gamma$. Whether this is a long or short time on the scale of generations depends primarily on γ/r^* ; it is long if relative fluctuations are small ($\sigma_r/r^* \ll 1$), or if the environmental timescale is much shorter than generation times ($\tau \ll 1/r^*$). Remarkably, a community of $S = 10^4$ 000

species would only need twice the time to reach few-species dominance as a 100-species community, all else being equal. Because $t_c \sim \gamma^{-1}$, we will refer to γ as the *rate of (stochastic) exclusion*.

Numerical simulations reveal transient diversity

In the absence of fitness fluctuations, the total abundance has a carrying capacity of $K = r^*/\mu$. By rescaling abundances, we can set $K = 1$. We measure time in units of $1/r^*$, approximately equal to one generation time, which we set to 1 day for ease of communication and without loss of generality. In addition to S , this leaves three non-dimensional parameters: $\sigma_r/r^*, \tau r^*, n_{\text{ext}}/K$.

[Figure 1](#) shows a simulation of Eq. (4). Starting from a perfectly even community ($n_i(0) = K/S, r_i(0) = r^*$) we observe that a handful of species become dominant in a few hundred days ([Figure 1C](#)). While it is difficult to judge any species' success by its instantaneous fitness ([Figure 1A](#)), the dominant species can be recognized as having the highest time-integrated fitness since the initial time ([Figure 1B](#)). Eventually, after a few thousand days, the community becomes dominated by a single species ([Figure 1D](#)). As we observe the abundances over long timescales—from years ([Figure 1C](#)), to decades ([Figure 1D](#)), to centuries ([Figure 1E](#)), to millennia ([Figure 1F](#))—the intervals between exchanges of dominance tend to lengthen. Correspondingly, species that are not dominant become increasingly rare, so that, for any positive extinction threshold n_{ext} , the number of extant species progressively decays until only one species remains (varying n_{ext}/K from 10^{-3} to 10^{-12} has less than an order of magnitude effect on the timescale of fixation; see [Figure 1D](#)). The last surviving species is at no practical risk of stochastic extinction, although, technically, it will vanish eventually.

We focus next on the timescale on which the community becomes highly uneven. As a proxy for the number of dominant species, we consider the *effective richness* (i.a. Simpson's reciprocal diversity index):

$$S_{\text{eff}}(t) := \frac{1}{\sum_i p_i^2(t)}, \quad (5)$$

where $p_i = n_i/N$ denote relative abundances. In the initially even community $S_{\text{eff}}(0) = S$, and $S_{\text{eff}} \rightarrow 1$ as monodominance appears at long times. We measure the time t_c at which the effective richness crosses a threshold of a few species. As shown in [Figure 2](#), uneven distributions readily emerge also in very large communities, with t_c scaling as $\ln S$.

The timescale t_c decreases with $\gamma = 2\sigma_r\tau$, as we prove in the next section. Indeed, γ essentially sets the 'ecological clock' of the model. As shown in [Figure 3](#), when γ is fixed, the other timescale parameter present, τ , has little effect on the main dynamical trends, but controls the extent of rapid fluctuations around them. These observations can justify modelling fitness fluctuations as white noise of amplitude $\sqrt{\gamma}$, but one should not conclude that time-correlations are unimportant, because, at the very least, they factor into the effective noise amplitude.

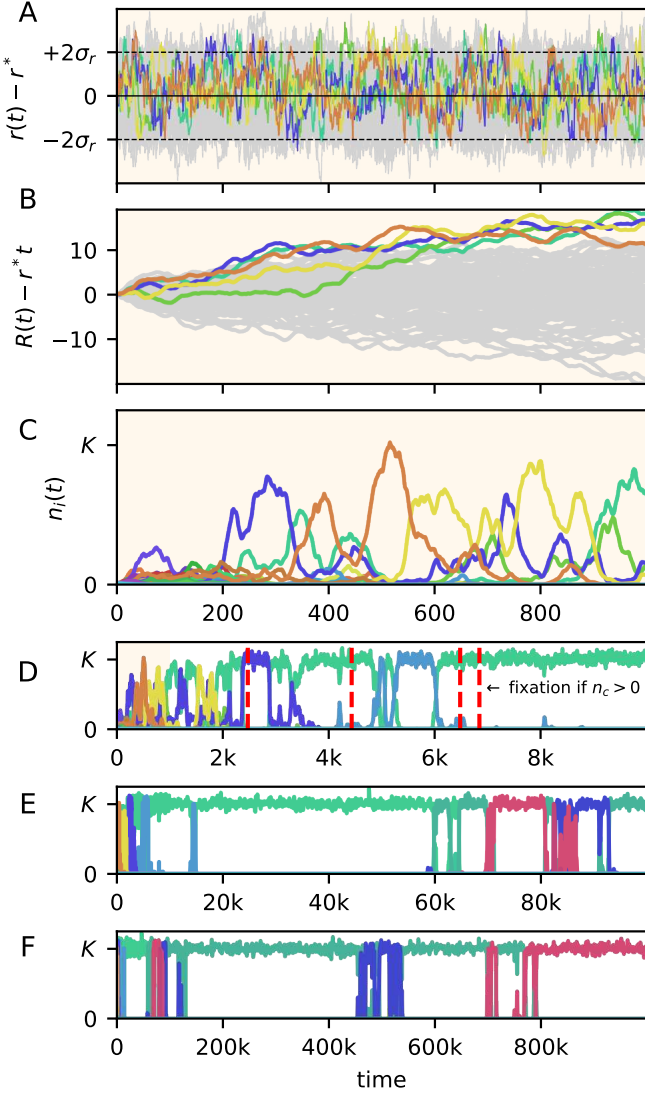


Figure 1: Simulated community dynamics showing progressive unevenness. Single simulation run of Eq. (1) & (3), starting from a perfectly even community. Instantaneous fitness (A) and time-averaged one (B), highlighted in colour for a few highly successful species. The same species are highlighted in the abundance time series (C-F), displayed in increasingly longer time windows. The simulation was run without an extinction threshold, but the vertical red lines in D indicate when, for the same fitness dynamics as shown, a single species would fixate under different extinction thresholds ($n_{\text{ext}}/K = 10^{-3}, 10^{-6}, 10^{-9}, 10^{-12}$). Despite a transient with high species diversity, monodominance is readily attained and is fixed for any positive extinction threshold. Simulation parameters are $S = 100$, $K = 1$, $r^* = 1$, $\gamma = 0.05$ $\tau = 10$.

A mapping to the replicator equation explains the dynamics of community unevenness

Despite the large fluctuations of individual species abundances in the simulation, the total abundance $N(t)$ fluctuates only moderately. This motivates focussing on the relative abundances $p_i = n_i/N$, which obey the replicator equation [55] (Appendix C)

$$\dot{p}_i(t) = p_i(t)[r_i(t) - \rho(t)], \quad (6)$$

where the mean fitness $\rho(t) := \sum_j r_j(t)p_j(t)$. This result follows from Eq. (1) regardless of the form of the $r_i(t)$'s, and is in fact independent of the neutral competition term $\mu N(t)$

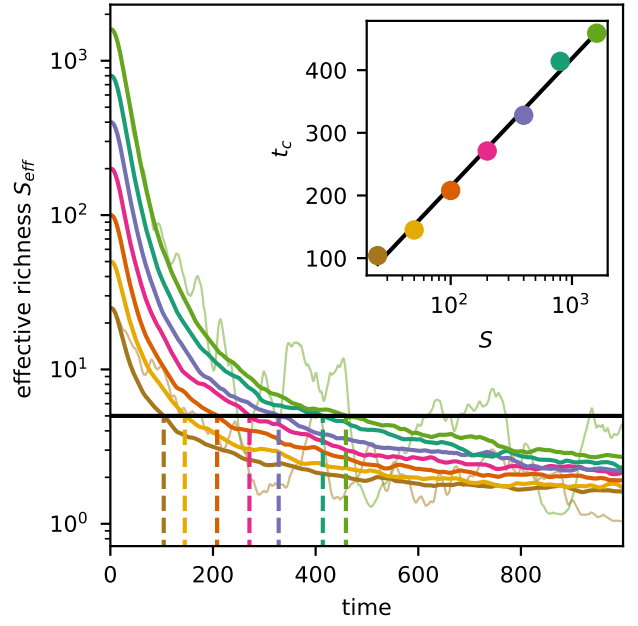


Figure 2: Decay of the effective species richness $S_{\text{eff}}(t)$ (Eq. (5)), starting from initially even community of 25 to 1600 species. Thick lines show averages over 200 simulations, with the two thin lines illustrating representative single runs for $S = 25$ and 1600. The inset shows the time t_c at which the ensemble-averaged $S_{\text{eff}}(t)$ has decayed to 5 species, plotted against the initial richness. The initially even community loses its diversity on a timescale of $\ln S$, in agreement with our calculations.

or its generalization to any function $g(n_1, \dots, n_S; r_1, \dots, r_S; t)$ that has the same value for all species. On the other hand, the strength of neutral competition constrains the total abundance, whose dynamics

$$\dot{N}(t) = N(t)[\rho(t) - \mu N(t)] \quad (7)$$

is only coupled to the species composition via the mean fitness.

Key to understanding the dynamics of species composition are the time-integrated fitnesses

$$R_i(t) := \int_0^t dt' r_i(t'), \quad (8)$$

as appreciated from the formal solution to Eq. (6):

$$p_i(t) = \frac{p_i(0)e^{R_i(t)}}{Z(t)}, \quad Z(t) := \sum_{j=1}^S p_j(0)e^{R_j(t)}. \quad (9)$$

A species i becomes dominant when the factor e^{R_i} makes up a sizeable fraction of the sum of exponentials, so that the question of dominance is essentially one of extreme value statistics. If the gap between the largest (or largest few) R_i and the rest tends to grow in time, then eventually—and, indeed, rather soon due to the exponentiation—the corresponding species will come to dominate. If species differ in their expected fitnesses, that with larger average fitness eventually wins deterministically (competitive exclusion). In the time-averaged neutral case with random fitness fluctuations following Eq. (3), after a transient of length com-

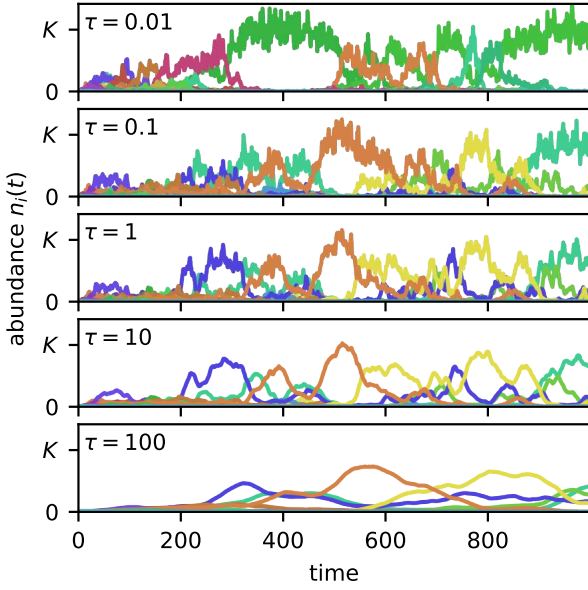


Figure 3: The main trend in community composition is scarcely affected by the fitness autocorrelation time τ —as long as γ is constant. The random numbers underlying the simulations are identical for all panels. We have fixed $\gamma = 0.05$, and set $\sigma_r = \sqrt{\gamma/2\tau}$. Other parameters as in Figure 1.

parable to τ , the R_i s diverge at rate γ (see Eq. (22) in Appendix A), which thus controls the speed at which community unevenness develops. The aging dynamics observed for $n_{\text{ext}} = 0$, where changes in dominance become increasingly rare, is also explained by the property of Brownian motions W_i to their origin in finite time despite the growing variance. These properties are not satisfied, for instance, when fluctuations are perfectly periodical, e.g. $r_i(t) = r^* + \sqrt{2}\sigma_r \cos(t/\tau - \phi_i)$. The variance among R_i s would remain bounded in this case, and no asymptotic monodominance would be established.

We note that Eq. (9) has the form of the Boltzmann distribution from equilibrium statistical physics. Indeed, in Appendix E we show how the ecological model with Gaussian fitness fluctuations can be exactly mapped to the ‘random energy model’ of a spin glass, for which many properties have been calculated in the large-system limit [56]. The spin glass exhibits a condensation phase transition at a critical temperature, which is mathematically analogous to the community unevenness transition at a critical time

$$t_c \sim \frac{\ln S}{\gamma}, \quad (10)$$

assuming $\tau \ll t_c$. (More generally, see Eq. (38).) This explains the simulation results in Figure 2.

The dynamics of community unevenness can also be understood through a focal species. For a community of two species [30], using $p_2 = 1 - p_1$ in Eq. (6),

$$\dot{p}_1(t) = \Delta r_1(t) p_1(t) [1 - p_1(t)], \quad (11)$$

with $\Delta r_1(t) := r_1(t) - r_2(t)$, which is independent of any species’ abundance. As the relative abundance of the focal species 1 approaches either 0 or 1, the dynamics slows

down, keeping the species generally closer to these extremes rather than at any intermediate value. We show in Appendix D that Eq. (11) holds for a focal species also in an S -species community, given a generalized form of Δr_1 . Consider the sub-community of all species *except* the focal one, and denote by $\rho_{\setminus 1}(t)$ the mean fitness in this subcommunity (i.e., where relative abundances are normalized only with respect to the $S - 1$ non-focal species). Then Eq. (11) holds for

$$\Delta r_1(t) := r_1(t) - \rho_{\setminus 1}(t). \quad (12)$$

Unlike the two-species case, Δr_1 now has a negative bias: $\rho_{\setminus 1}$ is weighted towards the species with higher abundances, which tend to have a higher-than average growth rate. Thus, all species are biased towards rarity, but the conservation of the total fraction (enforced by the correlations between all the Δr_i s) implies that some (ultimately only one) species will counter this tendency and reach a large fraction of the total population size.

Species loss is drastically slowed by intra-specific limitation or metacommunity buffering

As we have demonstrated, environmental stochasticity can drive ‘commonness of rarity’ and transient turnover of composition. The maintenance of species richness, however, requires local coexistence mechanisms [57, 58], or extinction–colonization balance [19, 59]. We therefore consider the effects of additional intraspecific limitation or metacommunity dispersal on diversity.

We suppose intraspecific competition exceeds interspecific competition by an amount $\varepsilon > 0$:

$$\dot{n}_i(t) = n_i(t)(r_i(t) - \mu N(t) - \varepsilon n_i). \quad (13)$$

This introduces negative frequency dependence, such that a species is penalized (favoured) when its relative abundance is above (below) $1/S_{\text{eff}}$ (see Eq. (51), Appendix G). In a suite of simulations in Figure 4A, we find that increasing ε/μ from 0 to 1 increases the timescale of substantial loss of species richness by many orders of magnitude. The effective species richness remains roughly constant until constrained by the absolute richness, as the rare species headed toward extinction have a marginal effect on the rest of the community. It is therefore reasonable to consider the community as quasi-stationary on timescales that can indeed be very long even when intraspecific suppression is weak. Further increasing ε/μ to around $3S\sigma_r/r^*$ ($= 15$ with default simulation parameters) would allow essentially all species to coexist deterministically if the fitnesses were suddenly frozen, i.e. drawn statically from the stationary distribution (Appendix F); then stochastic exclusion does not occur at all, in practise.

Alternatively, we add self-consistent dispersal among M patches:

$$\dot{n}_{i,\alpha} = n_{i,\alpha}(r_{i,\alpha} - \mu N_\alpha) + \sum_{\beta=1}^M (d_{\alpha\beta} n_{i,\beta} - d_{\beta\alpha} n_{i,\alpha}). \quad (14)$$

Naturally, the rates of local and regional extinction will depend on the number of patches and the topology of the network, the correlation in environmental conditions between

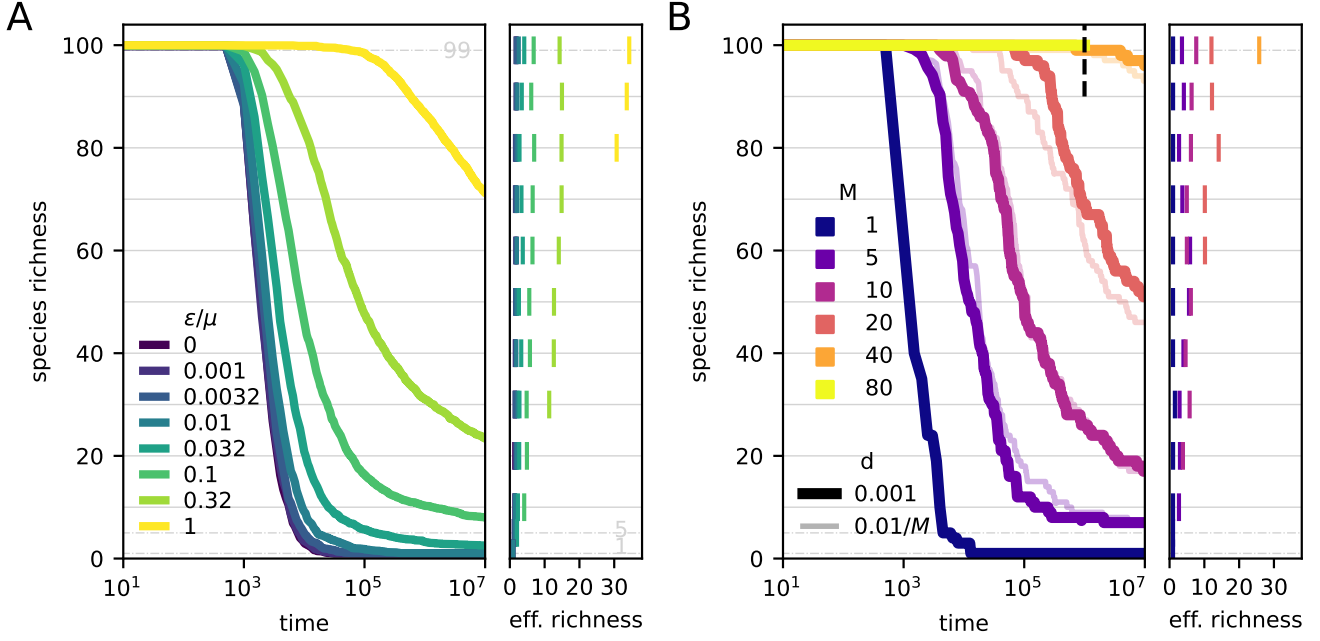


Figure 4: Loss of species richness (large panel) and effective richness Eq. (5) (side panel) over time. The effective richnesses are plotted for the times at which the absolute abundance crosses the level values indicated by horizontal grey lines. The average diversity decay over 20 simulation runs is plotted for different values of intra-specific suppression ε (A), and in metapopulations with different number of patches M and migration rates d (B). Other parameters are as given in Figure 1 with $n_{\text{ext}}/K = 10^{-12}$.

patches, the rates of dispersal, and the extinction threshold; enough factors to make a systematic analysis challenging. In Figure 4B we only consider a fully connected patch network, uncorrelated fitnesses, and vary either the net dispersal rate (d) or the dispersal per patch (d/M). In either case, every doubling of the number of patches leads to about one more order of magnitude in the time it takes to lose species richness in a given patch. Indeed, related metacommunity models have found species lifetimes to grow exponentially in the number of patches [25, 40].

Given the radical slowdown of diversity loss achievable by modest amounts of stabilization or buffering, we consider in the following the single-patch dynamics Eq. (1) without extinction cut-off, which has a true stationary state thanks to the constant immigration term λ . However, beyond promoting coexistence, the parameter ε and the immigration rate λ have pronounced effects abundance distributions, as we explore next.

A modified power-law abundance distribution is maintained by turnover of rare and dominant species

With Eq. (1) at hand, for which fitness fluctuations drive community unevenness but intraspecific suppression and immigration limit species rarity, we now look at two empirically relevant statistics: the abundance distributions displayed by individual species over long stretches of time (frequency–abundance distribution, FAD), or by all species of the community at a snapshot in time (species–abundance distribution, SAD). Their relation is illustrated in Figure 5A. While all species fluctuate in abundance over time, the SAD retains the same shape across snapshots, which appears to be a subsampling of the FAD. Moreover, all species have

identical FAD if compared for a sufficiently long time, due to species-symmetry of the model parameters. Thus, for large, time-average neutral communities, we think of the FAD and SAD as interchangeable.

To estimate the shape of these distributions we consider, similar to [43], an effective equation that governs the dynamics of a single, focal species:

$$\dot{n} = n(r_{\text{eff}}(t) - \varepsilon n) + \lambda. \quad (15)$$

Here, $r_{\text{eff}}(t)$ is again an Ornstein-Uhlenbeck process like Eq. (3), with statistics now chosen to approximate those of $r_i(t) - \mu N(t)$. Thus, we set the mean of the effective fluctuations to

$$r_{\text{eff}}^* = r^*(1 - \bar{N}/K), \quad (16)$$

with the over bar denoting an average over long times; the variance (neglecting the covariance of focal species fitness and total abundance) to

$$\sigma_{r_{\text{eff}}}^2 \approx \sigma_r^2 + \mu^2 \text{Var}[N]; \quad (17)$$

and $\tau_{\text{eff}} \approx \tau$, because fluctuations are chiefly driven by $r_i(t)$. In the fast-environment limit, where $\tau_{\text{eff}} \rightarrow 0$ while $\gamma_{\text{eff}} = 2\sigma_{r_{\text{eff}}}^2 \tau_{\text{eff}}$ remains finite, the stationary distribution is

$$P(n) \propto n^{-\nu} e^{-\frac{2}{\gamma_{\text{eff}}}(\varepsilon n + \lambda/n)}, \quad (18)$$

combining a power-law section with exponent

$$\nu = 1 - \frac{2r_{\text{eff}}^*}{\gamma_{\text{eff}}} \quad (19)$$

with cut-offs at low and high abundance set by immigration and self-suppression, respectively (abundances cannot

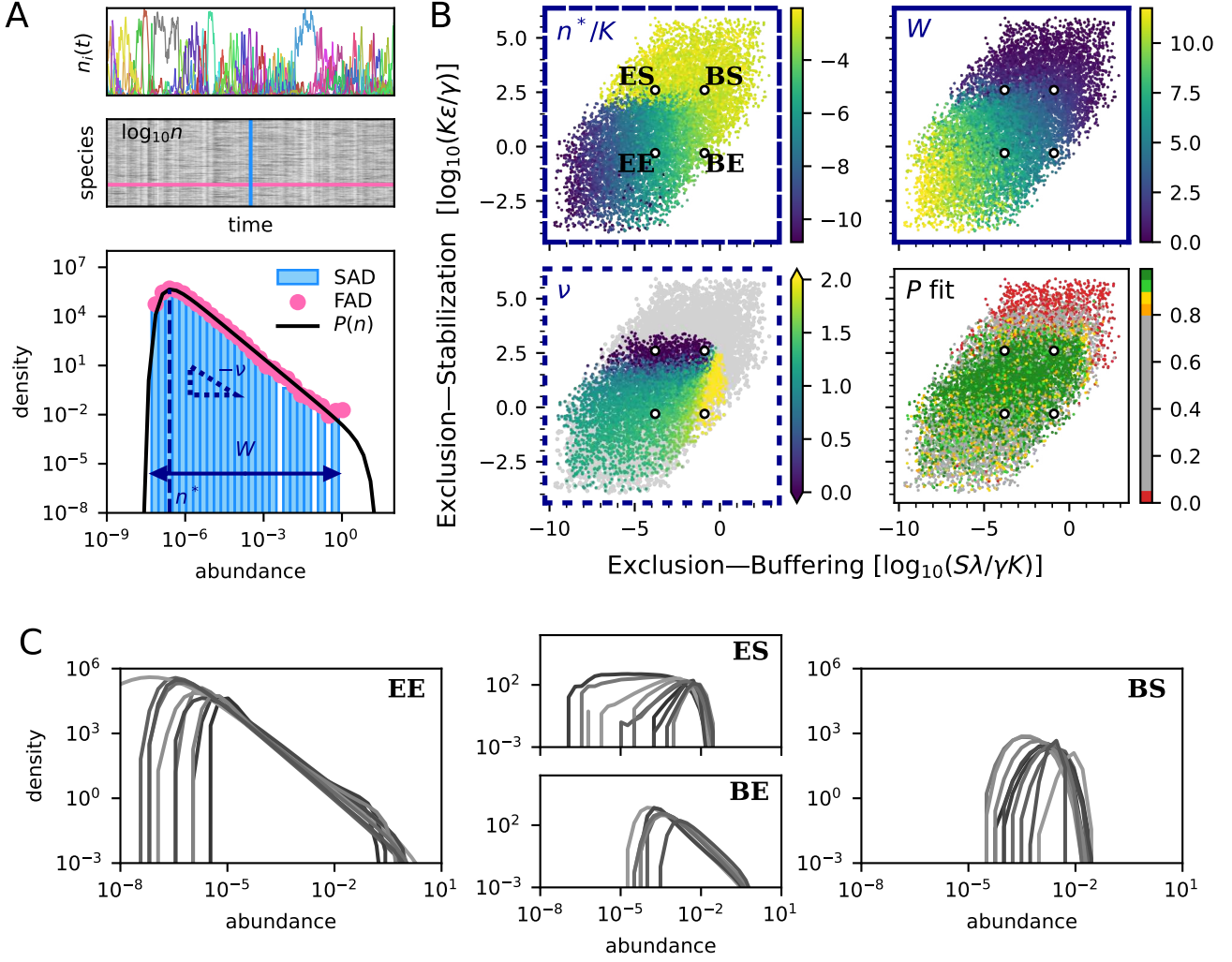


Figure 5: Variation in the shape of abundance distributions across simulated communities with varying base parameters. **A** An example times series (top) with the corresponding data matrix (middle). Different abundance distributions (bottom) can be constructed from this data: the ‘snapshot’ species abundance distribution (SAD, blue histogram); the frequency abundance distribution (FAD, pink symbols) for one arbitrary species. The black line denotes the predicted stationary distribution Eq. (53a) of the focal species model, parameterized with r_{eff}^* , $\sigma_{r_{\text{eff}}}$ as per the statistics of N in the simulation. Three key features of the distributions are highlighted in dark blue: the number of decades W spanned by the SAD; the modal abundance class n^* ; and the downward slope of the power-law section, as defined by the formula Eq. (19). **B** Variation of the highlighted features along the Exclusion–Stabilization and Exclusion–Buffering axes. Each point represents one simulation. Parameters are sampled (log-)uniformly to vary over orders of magnitude: $S \in [100, 1000]$, $\log_{10} \gamma \in [-4, 2]$, $\log_{10} \tau \in [-2, 2]$, $\log_{10} \epsilon \in [-2, 2]$, $\log_{10} \lambda \in [-10, 4]$. Units are adapted so that $K = 1$ and $r^* = 1$. Effective parameters appear to capture most of the shape variation, which is also reproduced by the focal species stochastic model. The goodness of fit of $P(n)$ with the species-averaged FAD (from 0 (no match) to 1 (perfect match)) is measured by (one minus) the Kolmogorov-Smirnov distance of the distributions: $1 - \sup_n |F_P(n) - F_{\text{FAD}}(n)|$. The predicted exponent is shown in colour only for simulations where the fit was $\geq 85\%$ accurate and the distribution with was at least two decades ($W \geq 2$). Note that colour scale for the exponent is capped in the range $[0, 2]$, so that all negative values appear in the same color (dark purple). **C** Examples of typical shapes of the abundance distributions. The species-averaged FAD is plotted for the 10 simulations whose parameters put them closest in the EB/ES plane to the four points labelled EE, ES, BE, BS in **B** (the two letters signifying the dominant end of the two axes). Differences in line colour are only a guide for the eye.

be smaller than $\sim \lambda$ and larger than $\sim 1/\epsilon$; see Appendix H. There, we also give an approximate solution for finite τ_{eff} , Eq. (53a), which has modified cut-offs but the same power law section compared to Eq. (18). Note that ν can be both larger and smaller than one, depending on the sign of r_{eff}^* .

How the shape of the distribution depends on the base parameters (i.e. $S, r^*, K = r^*/\mu, \gamma, \tau, \epsilon, \lambda$) is not fully clear from the focal-species model, as they enter indirectly in the effective rates r_{eff}^* , γ_{eff} and the three relevant parameter combinations $r_{\text{eff}}^*/\gamma_{\text{eff}}$, $\epsilon/\gamma_{\text{eff}}$, $\lambda/\gamma_{\text{eff}}$ that appear in Eq. (18). Going back to the full-community model, a dimensional analysis (Appendix G) indicates that most of the variation in distribution shape can be reduced to only *two* parameter com-

binations, that capture the *relative proportions* of exclusion rate, self-limitation rate, and total immigration rate. First, we make these three rates comparable by expressing them in our chosen units ($1/r^*$ for time, K for abundance):

$$\hat{\gamma} = \frac{\gamma}{r^*}, \quad \hat{\epsilon} = \frac{K\epsilon}{r^*}, \quad \hat{\lambda}_{\text{tot}} = \frac{S\lambda}{Kr^*}. \quad (20)$$

From these, we choose two log-ratios (since the third log-ratio is fully determined by the other two): we call $\log(\hat{\epsilon}/\hat{\gamma})$ the *Exclusion–Stabilization axis*, and $\log(\hat{\lambda}_{\text{tot}}/\hat{\gamma})$ the *Exclusion–Buffering axis*.

To see how the distribution varies along these axes we simulate 10'000 communities with base parameters drawn

randomly from a wide range of values. We quantify the distribution shape by three indices (illustrated in Figure 5A)—the width W in number of abundance decades; the most-common abundance n^* ; and the power-law exponent ν as predicted by Eq. (19)—and confirm that the ES and EB axes account for most of the observed variation (Figure 5B). The shape changes continuously between a few qualitatively different limit cases. Figure 5C and additional plots in Supplementary Figure 1 are illustrative of four regions in the ES/EB plane.

When exclusion dominates over both buffering and suppression, the distribution is characterized by a power-law section spanning many orders of magnitude (Figure 5C, point EE). A few species are highly dominant, and the majority are rare. In the absence of a lower abundance threshold set by immigration, fluctuations would drive an ever-widening power law of exponent approaching 1 (Supplementary Figure 2; see also the Poisson-process limit law [60]). Increasing the relative importance of buffering (moving from point EE to BE), the general shape of the distribution is retained, but its support narrows. As a consequence, the power-law section becomes steeper. If stabilization is instead increased (moving from point EE to ES), the mode of the distribution drastically shifts from lying close to the immigration threshold to approaching the single-species carrying capacity (which is simultaneously reduced by self-limitation). This shift coincides with the power-law exponent changing sign. When it is positive, the shape resembles a gamma distribution (with a far-left cutoff due to immigration). Moving equally up the ES and EB axes (from EE to BS; e.g., by increasing $\hat{\varepsilon}$ and $\hat{\lambda}_{\text{tot}}$ in equal measure, or only decreasing $\hat{\gamma}$), the support of the distribution narrows, and its shape resembles a log-normal distribution.

When, as here, the SAD reflects an FAD common to all species, its shape is closely linked to temporal beta diversity—measurable from ecological time series [61]. The average Bray-Curtis similarity $BC(t)$ of communities observed a time t apart decays from 1 towards a limiting value that depends on the shape of the distribution, thus chiefly on the position in the EB/ES plane (Supplementary Figure 3). Indeed, comparing the community composition at two time points sufficiently far apart amounts to randomizing the species ranks of the second sample with respect to the first, while preserving the SAD. For the power-law shape in the exclusion-dominated region, the asymptotic similarity is smaller than when abundances are more narrowly distributed around their mode (< 0.15 compared to > 0.5). The rate at which BC similarity decays, however, depends on the actual value of the exclusion rate γ . For large γ , specifically, the dominance of exclusion is associated to a faster species turnover and larger abundance fluctuations.

Heterogeneous fitnesses create persistent biases in species rarity

Finally, we relax the assumption of time-averaged neutrality in order to test the robustness of our results when species within the same community differ in their long-term abundance statistics, as expected in real ecosystems.

We take two reference parameter sets, corresponding to the exclusion-dominated and stabilization- and buffering-dominated regions of the EB/ES plane (EE and BS, respectively, in Figure 5B,C). For each case, we draw the species-specific fitness averages r_i^* from a uniform distribution in the range $r^* \pm \delta r^*$, but keep other parameters ($\sigma_r, \tau, \varepsilon, \lambda$) identical for all species. The fitness distributions are now same-width normal distributions with different means; how much they overlap is controlled by $\delta r^*/\sigma_r$, which we vary from 0 to 10. As this ratio increases, the species-specific FADs separate, and species of lower (higher) r_i^* become biased towards rarity (dominance); Figure 6. For the heavy-tailed distribution in the EE case, the time-averaged SAD (coinciding by definition with the species-averaged FAD) changes little during this splitting. For the BS case, the bell-shape average SAD widens to eventually develop a power-law trend. The breaking of TAN also leads to a smaller turnover as measured by the BC index limit, as species become more constrained in their fluctuations, whether biased towards rarity or dominance (Supplementary Figure 4).

Focussing on the emerging species differences, we note that a spread in mean fitness within the limits of a doubling/halving of the average (the rightmost panels of Figure 6 have $r_i^* \in [0.5, 1.5]$) is able to produce a distribution of species mean abundances spanning several orders of magnitude (Supplementary Figure 5). The shape of the FADs can also differ between species. As FADs split, the ‘frequent’ species’ FADs are more gamma-like, whereas ‘infrequent’ ones have a longer right tail, as particularly evident in the SB example. The possible FAD shapes of different species are still described by the focal-species model Eq. (15), but now the species have different r_{eff}^* , set by $r_i^* - \mu\bar{N}$. Thus, based on its expected fitness, a species may be relatively more or less constrained by immigration or self-limitation.

DISCUSSION

We used a minimal model encompassing environmental stochasticity, intra- and inter-specific competition, and dispersal to relate three features of natural communities: the coexistence of many species, the ‘commonness of rarity’, and species turnover.

Even if every species has the same time-averaged fitness, random fitness fluctuations drive the community toward ever-greater unevenness (and species extinctions), unless countered by other processes. Contrary to strictly neutral dynamics driven by demographic noise [28], the timescale on which a few species rise to dominance is independent of total carrying capacity [50]. Its determinants are the variance of fitness fluctuations and their correlation time (combined in a parameter we called the exclusion rate, γ), beside a weak dependence on the number of species in the community. While the community eventually settles into monodominance, the transient dynamics may resemble real community time series over a span of many generations [48]. However, unlike for asymptotic dynamics, statistics on transient states inherently depend on the initial condition.

Steady states with high species diversity emerge instead

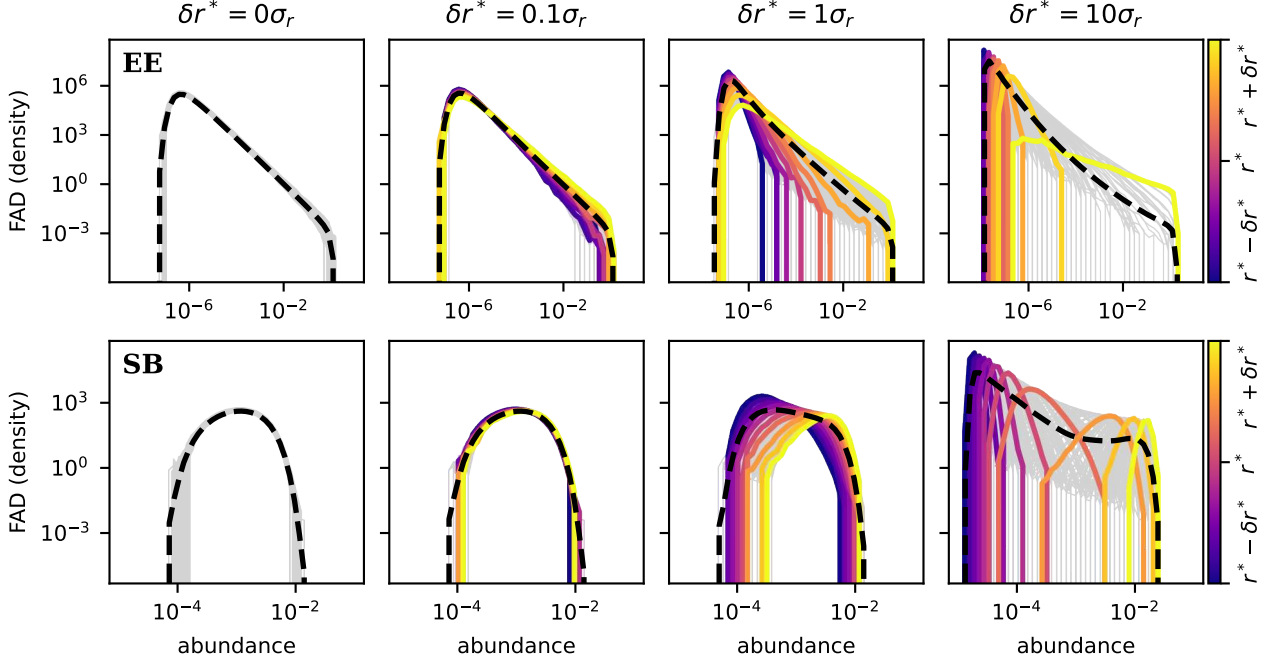


Figure 6: Emergence of frequent and infrequent species under breaking of time-averaged neutrality. The two rows report the same numerical protocol but starting from different sets of model parameters, corresponding to the scenarios EE and BS in Figure 5. Time-averaged neutrality is broken by drawing the r_i^* s uniformly at random from the interval $[r^* - \delta r^*, r^* + \delta r^*]$, with δr^* varying by column. In each panel, the frequency–abundance distribution (FAD) of each individual species is plotted, with a subset of species shown in colour according to their r_i^* ; the black dashed lines are the species-averaged FADs (equal to the time-averaged SAD). Simulation parameters used are $S = 500$, $r^* = 1$, $\mu = 1$, $\sigma_r = 0.05$, $\tau = 10$, and for EE, BS, respectively, $\varepsilon = 0.05, 50$; $\lambda = 10^{-8}, 3.2 \times 10^{-5}$. Simulations were run for 500'000 time units.

from a combination of local coexistence mechanisms and extinction-colonization balance. We observed how increasing intraspecific competition (implying stabilization through niche-differentiation [62]), or introducing dispersal within a metacommunity (promoting a spatiotemporal buffering effect [23, 25]) can preserve both absolute and effective species richness on super-generational timescales. We thereafter focussed on the abundance dynamics in a single patch with both intra-specific limitation and constant immigration.

By changing the model parameters, the dynamics exhibits different regimes with characteristic community patterns. To understand the variation in shape of the species–abundance distribution (SAD), in particular, we exploited its correspondence to the frequency–abundance distribution (FAD) of single species when the community is species-rich and time-average neutral. A focal-species model predicts the functional form of the distribution, but depends on effective parameters whose values are not *a priori* known. However, the distribution shape ends up being predominantly controlled by the relative rates of stochastic exclusion, self-limitation, and total immigration, summarized in an Exclusion–Buffering and Exclusion–Stabilization (EB/ES) plane. Its axes are similar in spirit to niche–neutral and dispersal-limitation axes [31–33, 63], but stochastic exclusion results here from environmental fluctuations as opposed to neutral drift.

We described the patterns of unevenness and turnover found across the EB/ES plane. When stochastic exclusion dominates, there are a few dominant (or even hyper-dominant [48, 49]) species at any given time, while the rare

species are maintained by immigration. Concomitantly, there is high turnover of species between the dominant and rare component. The SAD is characterized by an extended power-law section between the immigration threshold and the single-species carrying capacity, similar to what observed in plankton communities [13]. A ‘power bend’ (a power-law decay with exponential cutoff) appears to be a commonly good fit to empirical SADs [11], with exponents close to 1 for animals and plants, and with a median of 1.6 in microbial communities—a range encompassed by our results. As stabilization becomes stronger in the model, the SAD comes to resemble a gamma distribution, which has been associated with FADs in various microbial communities [64, 65]. Increasing also immigration leads to a more classical log-normal-like shape [4], associated with more stable community compositions, and less rapid turnover.

Time-average neutrality is a useful hypothesis for a null model, but is likely unrealistic. We have therefore introduced heterogeneity in mean fitnesses, and observed the emergence of persistently common or rare species, with a split in both the shapes and locations of the FADs. This distinction reflects a difference in temporal occurrence, reminiscent of the distinction, in natural communities, between ‘core’, endemic species and ‘occasional’ species, which are less systematically sampled [66]. Although the SAD now does not necessarily look like the FAD of any particular species, the individual FADs can still be described by the same focal-species model but with different effective parameter values. Incorporating in the same focal-species framework alternative hypotheses on species heterogeneity, e.g. differences in intraspecific [67, 68] or interspecific compe-

tition [43, 69, 70], would be an interesting extension of this work.

In fact, at the focal species level, different community dynamical hypotheses seem to converge. For example, dynamical models proposed to explain a suite of co-occurring patterns in microbial communities [64, 65, 71–74] have differed in the emphasis on species interactions [73], parameter heterogeneity [64], or spatiotemporal coarse-graining [74] but all stress the importance of effectively random growth rate fluctuations. More broadly, the multitude of reasons for communities to be complex and out of equilibrium may through a funnel of effective stochasticity underlie common diversity patterns.

With the deployment of systematic observational studies, communities are characterized with increasing time resolution. Integration of classical community statistics obtained at fixed time (like SADs) with time-series of single species then can pave the way to distinguishing ecological regimes and their key driving processes. This effort, beyond the identification of which model best accounts for an observed pattern, is essential for deciding how to detect shifts in the dynamics of natural communities and preserve their diversity.

ACKNOWLEDGEMENTS

The authors thank Nadav Shnerb and David Kessler for insightful discussions and sharing [49] ahead of publication.

APPENDIX

A Statistics of fitness fluctuations

Integrating the Ornstein-Uhlenbeck process, Eq. (3), from time t_k to $t_{k+1} = t_k + \Delta t$ (dropping the index i for brevity),

$$r(t_{k+1}) = r(t_k)e^{-\Delta t/\tau} + r^*(1 - e^{-\Delta t/\tau}) + \sigma_r u(\Delta t/\tau) X_k, \quad (21)$$

where $X_k \sim \mathcal{N}(0, 1)$ and $u(s) = \sqrt{1 - e^{-2s}}$. The integrated fitness satisfies [75]

$$R(t_{k+1}) = R(t_k) + r^* \Delta t + \tau(r(t_k) - r^*)(1 - e^{-\Delta t/\tau}) + \sqrt{\gamma \Delta t} v(\Delta t/\tau) Y_k, \quad (22)$$

where $Y_k \sim \mathcal{N}(0, 1)$ and

$$v(s) = \sqrt{1 - \frac{1}{2s}(3 + e^{-2s} - 4e^{-s})} \sim \begin{cases} \frac{1}{\sqrt{3}}s & s \ll 1 \\ 1 & s \gg 1 \end{cases}. \quad (23)$$

Note that X_k, Y_k have a correlation $C(\Delta t/\tau)$ with

$$C(s) = \frac{1 - 2e^{-s} + e^{-2s}}{\sqrt{(1 - e^{-2s})(2s - (3 + e^{-2s} - 4e^{-s}))}}, \quad (24)$$

which is also the correlation between $R(\Delta t)$ and $r(\Delta t)$. It takes $t \approx 50\tau$ for $C(t/\tau)$ to reduce from $C(0) = \sqrt{3}/2$ to a 10% correlation, and 5000τ to a 1% correlation.

B Numerical integration

The numerical integration of Eq. (1) was done with the scheme

$$n_i[t + \Delta t] \leftarrow n_i[t] \exp\{\Delta R_i[t] - \Delta t(\mu N[t] + \varepsilon n_i[t])\} + \lambda \Delta t. \quad (25)$$

It ensures positivity of abundances, and, if $\varepsilon = 0$ and $\lambda = 0$, reproduces the analytically exact path probabilities for relative abundances regardless of step size Δt . A step-size of $\Delta t = 0.01$ was used throughout. For Ornstein-Uhlenbeck noise, ΔR_i can be sampled from Eq. (22) in tandem with Eq. (21), involving no approximations.

In the metacommunity version of the model Eq. (14),

$$n_{i\alpha}[t + \Delta t] \leftarrow \left(\sum_{\beta=1}^M n_{i\beta}[t] \mathcal{D}_{\beta\alpha} \right) \times \exp\{\Delta R_{i\alpha}[t] - \Delta t(\mu N_\alpha[t] + \varepsilon n_{i\alpha}[t])\}, \quad (26)$$

where

$$\mathcal{D}_{\alpha\alpha} = 1 - e^{-d_\alpha \Delta t}, \quad \mathcal{D}_{\alpha\beta} = \frac{d_{\beta\alpha}}{d_\alpha} e^{-d_\alpha \Delta t} \quad (\beta \neq \alpha). \quad (27)$$

C Derivation of the replicator equation

To derive Eq. (6)–(7) from Eq. (1), consider more generally

$$\dot{n}_i(t) = n_i(t)[r_i(t) - g(\mathbf{n}(t), \mathbf{r}(t), t)]. \quad (28)$$

By summing over i we get immediately

$$\dot{N}(t) = N(t)[\rho(t) - g(\mathbf{n}(t), \mathbf{r}(t), t)], \quad (29)$$

with $\rho = \sum_j r_j n_j$. Applying the chain rule to $p_i = n_i/N$,

$$\dot{p}_i = \frac{\dot{n}_i}{N} - p_i \frac{\dot{N}}{N} = \frac{n_i}{N}(r_i - g) - p_i(\rho - g) = p_i(r_i - \rho). \quad (30)$$

The cancellation of g hinges upon it being identical for all species (i.e. neutral).

D Derivation of focal-species replicator equation

Here we derive the focal-species Eq. (11) revealing the stickiness effect. With p_i , $i = 1, \dots, S$, the relative abundances in the full community, define the relative abundance $p_{i \setminus 1}$, $i = 2, \dots, S$, in the sub-community excluding species 1:

$$p_{i \setminus 1} := \frac{n_i}{\sum_{j=2}^S n_j} = \frac{p_i}{1 - p_1}, \quad i > 1. \quad (31)$$

Note that $p_{i \setminus 1}$ is independent of the fitness of species 1 since

$$p_{i \setminus 1} = \frac{p_i(0)e^{R_i}}{\sum_{j>1} p_j(0)e^{R_j}}. \quad (32)$$

The mean fitness in the full community is

$$\rho = p_1 r_1 + \sum_{i=2}^S p_i r_i = p_1 r_1 + (1 - p_1) \rho_{\setminus 1}, \quad (33)$$

where we have substituted $p_{i \setminus 1}(1 - p_1)$ for p_i according to Eq. (31), and identified

$$\rho_{\setminus 1} := \sum_{i=2}^S p_{i \setminus 1} r_i. \quad (34)$$

Substituting the above expression for ρ in the replicator equation, Eq. (6), for $i = 1$ produces Eq. (11) after some elementary algebra.

E Unevenness as a phase transition

Here we give more details on the derivation of the timescale of the unevenness transition, and the mapping to a spin glass.

At any fixed time t , the distribution of $p_i(t)$, Eq. (9), has the mathematical form of a Boltzmann distribution,

$$p_i^B = \frac{e^{-\beta E_i}}{Z^B}. \quad (35)$$

The S species correspond to as many configurations of some physical system, for instance the $S = 2^J$ possible configuration of J Ising spins, in contact with a heat bath at inverse temperature β . $\ln n_i(0) + R_i(t)$ is mapped to βE_i , with E_i the energy of the physical configuration. We assume fitness fluctuations according to Eq. (3); that $n_i(0)$ are log-normally distributed with log-variance $\sigma_{n,0}^2$; and that the $r_i(0)$ s are normal with variance $\sigma_{r,0}^2$. Then $\ln n_i(0) + R_i(t)$ is normally distributed at any $t \geq 0$. The assumption of normal energy levels with variance $J/2$ defines the celebrated random energy model (REM) of a spin glass [56, 76]. The mapping from the ecological model to the REM is fixed by choosing $\beta = \beta(t)$ according to

$$\beta^2 J/2 = \text{Var}[n(0) + R(t)], \quad 2^J = S. \quad (36)$$

In the ‘thermodynamic limit’ $J \rightarrow \infty$, the REM exhibits a condensation phase transition at the critical inverse temperature $\beta_c = 2\sqrt{\ln 2}$, separating a phase dominated by the energy ground state and one where almost all states are equiprobable. Thus, in the community model there is a dominance transition at the critical time t_c given implicitly by $\beta_c = \beta(t_c)$. From our assumptions, using Eq. (22),

$$\left(\frac{\beta(t)}{\beta_c}\right)^2 = \frac{1}{2 \ln S} \left(\sigma_{n,0}^2 + \tau^2(1 - e^{-t/\tau})^2 \sigma_{r,0}^2 + \gamma v^2(t/\tau) \right). \quad (37)$$

In the case of an initially even community, $\sigma_{n,0} = 0$, and initial fitnesses drawn from the stationary distribution, $\sigma_{r,0} = \sigma_r$, we have

$$\gamma t_c w^2(t_c/\tau) = 2 \ln S, \quad (38)$$

where

$$w^2(s) := \frac{(1 - e^{-s})^2}{s} + v^2(s) = \frac{e^{-2s} - (1 - 2s)}{2s}. \quad (39)$$

Using $w(s \gg 1) = 1$ and $w(s) = s + O(s^2)$,

$$t_c = \begin{cases} \frac{2 \ln S}{\gamma}, & \tau \ll t_c, \\ \frac{2 \ln S}{\gamma} \cdot \sqrt{\frac{\gamma \tau}{2 \ln S}}, & \tau \gg t_c. \end{cases} \quad (40)$$

Note, however, that the critical time should diverge in the large-community limit where the condensation phase transition becomes sharp; for finite communities the unevenness transition is therefore always observed as a smooth crossover of regimes.

For a heuristic derivation of Eq. (38), following [76], consider, at any given time, the variance in the normalization factor Z in Eq. (9) over many realizations of the fluctuating fitnesses: if it is large, that signals that the sum tends to be dominated by a few fluctuating terms. Denote $X_i(t) = \ln n_i(0) + R_i(t)$. The analysis is straightforward if the $X_i(t)$ are normal i.i.d. Then using $\mathbb{E}[e^{X_i}] = \exp\{\mathbb{E}[X_i] + \text{Var}[X]/2\}$,

$$\mathbb{E}[Z] = S e^{\mathbb{E}[X] + \frac{1}{2} \text{Var}[X]}, \quad (41)$$

$$\mathbb{E}[Z^2] = S e^{2\mathbb{E}[X]} (e^{2\text{Var}[X]} + (S-1)e^{\text{Var}[X]}); \quad (42)$$

hence, with $S-1 \approx S$,

$$\frac{\text{Var}[Z]}{\mathbb{E}[Z]^2} = e^{\text{Var}[X] - \ln S}. \quad (43)$$

As S becomes large, the Z -variance is non-negligible for times t large enough that the above exponent is not very negative; $\text{Var}[X(t)] \gtrsim \ln S$.

F Coexistence fixed point for fixed fitness values

We are solving for the fixed points of

$$\dot{n}_i(t) = n_i(t)[r_i - \mu N(t) - \varepsilon n_i(t)] = 0, \quad \varepsilon > 0, \quad (44)$$

where r_i are some fixed numbers. Let $s_i = 1$ if species i survives in the fixed point and 0 if it is extinct. Then its equilibrium abundance is

$$\hat{n}_i = s_i \frac{r_i - \mu \hat{N}}{\varepsilon}, \quad (45)$$

where $\hat{N} = \sum_{j=1}^S \hat{n}_j$. Summing Eq. (45) and solving for \hat{N} yields

$$\hat{N} = \frac{\hat{r}}{\mu + \varepsilon/\hat{S}}, \quad (46)$$

where $\hat{S} = \sum_{j=1}^S s_j$ and $\hat{r} = \sum_{j=1}^S s_j r_j / \hat{S}$. Thus

$$\hat{n}_i = s_i \frac{1}{\varepsilon} \left(r_i - \frac{\hat{r}}{1 + \frac{\varepsilon}{\mu \hat{S}}} \right). \quad (47)$$

Feasibility requires that $r_i > \hat{r}/(1 + \varepsilon/\mu \hat{S})$ if $s_i = 1$; uninvadability requires that $s_i = 1$ if this rate inequality holds. Stability of fixed points follows from the negative definiteness of the interaction matrix $[-\mu - \delta_{ij}\varepsilon]$; symmetric interactions preclude chaos or limit cycles [55]. Suppose $r_1 > r_2 > r_3 \dots$. One concludes that there is a unique uninvadable fixed point consisting of the species with the largest r_i , up to the largest index i for which $r_i > \sum_{j=1}^i r_j / (1 + \varepsilon/\mu i)$.

If the r_i were drawn from $\mathcal{N}(r^*, \sigma_r)$, then the smallest among S would be $r_S = r^* - h(S)\sigma_r$, where $h(S)$ is a random variable whose distribution for large S is known

from extreme value theory [77]. For $S = 100, 1000, 10000$, $\mathbb{E}[h(S)] \approx 2.5, 3.2, 3.9$, i.e. relatively insensitive to S . Thus, essentially all species coexist when

$$\frac{\varepsilon}{\mu} > S \left(\frac{1}{1 - h(S)\sigma_r/\hat{r}} - 1 \right) \approx 3S \frac{\sigma_r}{r^*}, \quad (48)$$

if σ_r/r^* is small.

G Dimensional analysis

Here we show which parameter combinations have qualitative effect on the model Eq. (1) & (3).

The special case Eq. (4) indicates that $1/\gamma$ (rather than $1/r^*$) is generally the natural timescale, and $K = r^*/\mu$ the natural scale of abundances. We therefore introduce the non-dimensional time $\tilde{t} := \gamma t$. We shift and rescale fitnesses as $\tilde{r}_i(\tilde{t}) := (r_i(t) - r^*)/\gamma$, and define $\tilde{W}(\tilde{t}) \sim \mathcal{N}(0, \tilde{t})$, to transform Eq. (3) into

$$(\tau\gamma) \frac{d}{d\tilde{t}} \tilde{r}_i = -\tilde{r}_i + \frac{d}{d\tilde{t}} \tilde{W}. \quad (49)$$

We derive evolutions for $\tilde{N}(\tilde{t}) := N(t)/K$ and $\tilde{p}_i(\tilde{t}) := p_i(t)$, similar to the derivation of Eq. (7) and Eq. (6) in Appendix C, obtaining

$$\frac{d}{d\tilde{t}} \tilde{N} = \frac{r^*}{\gamma} \tilde{N} \left[1 - \left(1 + \frac{K\varepsilon}{r^*} \frac{1}{\tilde{S}_{\text{eff}}} \right) \tilde{N} + \tilde{\rho} \right] + \frac{S\lambda}{\gamma K}, \quad (50)$$

and

$$\begin{aligned} \frac{d}{d\tilde{t}} \tilde{p}_i &= \tilde{p}_i [\tilde{r}_i - \tilde{\rho}] + \frac{K\varepsilon}{\gamma} \tilde{N} \tilde{p}_i \left(\frac{1}{\tilde{S}_{\text{eff}}} - \tilde{p}_i \right) \\ &\quad + \frac{S\lambda}{\gamma K} \cdot \tilde{N} \left(\frac{1}{S} - \tilde{p}_i \right), \end{aligned} \quad (51)$$

where $\tilde{\rho} := \sum_i \tilde{r}_i \tilde{p}_i$. As is to be expected, the set of equations (49)–(51) depend (beside S) on the full set of non-dimensionalized parameters

$$\tilde{\tau} := \gamma\tau, \quad \tilde{r}^* := \frac{r^*}{\gamma}, \quad \tilde{\varepsilon} := \frac{K\varepsilon}{\gamma}, \quad \tilde{\lambda}_{\text{tot}} = \frac{S\lambda}{\gamma K}. \quad (52)$$

However, Eq. (51) only has a *direct* dependence on $\tilde{\varepsilon}$ and $\tilde{\lambda}_{\text{tot}}$. So if \tilde{N} is relatively constant and τ not much larger than $1/\gamma$ we can expect the stationary distribution to depend mainly on $\tilde{\varepsilon}$ and $\tilde{\lambda}_{\text{tot}}$.

Note that non-dimensional parameters here (with a tilde) are different than those introduced in Eq. (20) (with carets), with the relations $\tilde{\varepsilon} = \hat{\varepsilon}/\hat{\gamma}$, $\tilde{\lambda}_{\text{tot}} = \hat{\lambda}_{\text{tot}}/\hat{\gamma}$.

H Stationary abundance distribution of the focal-species model

We consider here the stationary distribution of Eq. (15). This problem is not exactly solvable due to the noise being coloured but can be dealt with using a standard approximation (see SI of [43] for full derivation). The result is

$$P(n) = \frac{1}{\mathcal{N}} \left(\frac{1}{\tau_{\text{eff}}} + \varepsilon n + \frac{\lambda}{n} \right) n^{-\nu} \exp[-q_-(\varepsilon n) - q_+(\lambda/n)] \quad (53a)$$

$$\nu = 1 - \frac{r_{\text{eff}}^*}{\tau_{\text{eff}} \sigma_{r_{\text{eff}}}^2}, \quad q_{\pm}(x) = \frac{(x + \tau_{\text{eff}}^{-1} \mp r_{\text{eff}}^*)^2}{2\sigma_{r_{\text{eff}}}^2}. \quad (53b)$$

In the fast-environment limit ($\tau \rightarrow 0$ at fixed γ), we obtain Eq. (18) by keeping from the large parenthesis in Eq. (53a) only the constant diverging term, and expanding $q_{\pm}(x)$ to first finite order; apparent divergences of constants must cancel in the new normalization.

The normalization factor \mathcal{N} requires special care to evaluate numerically. Write Eq. (53a) as

$$P(n) = e^{\mathcal{H}(n) - \ln \mathcal{N}}, \quad (54)$$

and evaluate $\ln \mathcal{N}$ according to

$$\ln \mathcal{N} = \mathcal{L}^* + \ln \int_{-\infty}^{\infty} dy e^{\mathcal{L}(y) - \mathcal{L}^*} \quad (55)$$

where $\mathcal{L}(y) = \mathcal{H}(e^y) + y$ and $\mathcal{L}^* = \max_y \mathcal{L}(y)$. The integral appearing in Eq. (55) can be evaluated with standard numerical integration.

References

- [1] G. Hardin, The competitive exclusion principle, *Science* **131**, 1292 (1960).
- [2] G. E. Hutchinson, The paradox of the plankton, *Am. Nat.* **95**, 137 (1961).
- [3] S. A. Levin, Community equilibria and stability, and an extension of the competitive exclusion principle, *The American Naturalist* **104**, 413 (1970).
- [4] F. W. Preston, The commonness, and rarity, of species, *Ecology* **29**, 254 (1948).
- [5] B. J. Enquist et al., The commonness of rarity: global and future distribution of rarity across land plants, *Science Advances* **5**, 10.1126/sciadv.aaz0414 (2019).
- [6] H. ter Steege et al., Hyperdominance in the amazonian tree flora, *Science* **342**, 10.1126/science.1243092 (2013).
- [7] D. L. M. Cooper et al., Consistent patterns of common species across tropical tree communities, *Nature* **625**, 728 (2024).
- [8] T. J. Matthews and R. J. Whittaker, Fitting and comparing competing models of the species abundance distribution: assessment and prospect, *Frontiers of Biogeography* **6**, 10.21425/F5FBG20607 (2014).
- [9] B. J. McGill et al., Species abundance distributions: moving beyond single prediction theories to integration within an ecological framework, *Ecology Letters* **10**, 995 (2007).
- [10] L. H. Antão, A. E. Magurran, and M. Dornelas, The shape of species abundance distributions across spatial scales, *Frontiers in Ecology and Evolution* **9**, 10.3389/fevo.2021.626730 (2021).
- [11] Y. Gao, A. Abdullah, and M. Wu, A unifying model of species abundance distribution, *bioRxiv*, 10.1101/2024.06.14.599104 (2024).

- [12] J. Soininen, A quantitative analysis of species sorting across organisms and ecosystems, *Ecology* **95**, 3284 (2014).
- [13] E. Ser-Giacomi et al., Ubiquitous abundance distribution of non-dominant plankton across the global ocean, *Nature Ecology & Evolution* **2**, 1243 (2018).
- [14] C. M. Mutshinda, Z. V. Finkel, C. E. Widdicombe, and A. J. Irwin, Ecological equivalence of species within phytoplankton functional groups, *Functional Ecology* **30**, 1714 (2016).
- [15] T. L. Rogers, S. B. Munch, S. ichiro S. Matsuzaki, and C. C. Symons, Intermittent instability is widespread in plankton communities, *Ecology Letters* **26**, 470 (2023).
- [16] V. Smetacek, Making sense of ocean biota: how evolution and biodiversity of land organisms differ from that of the plankton, *Journal of Biosciences* **37**, 589 (2012).
- [17] M. Vellend, *The theory of ecological communities* (Princeton University Press, 2016).
- [18] B. J. McGill, The what, how and why of doing macroecology, *Global Ecology and Biogeography* **28**, 6 (2018).
- [19] S. P. Hubbell, *The unified neutral theory of biogeography* (Princeton University Press, 2001).
- [20] S. P. Hubbell, Neutral theory in community ecology and the hypothesis of functional equivalence, *Functional Ecology* **19**, 166 (2005).
- [21] I. Volkov, J. R. Banavar, S. P. Hubbell, and A. Maritan, Neutral theory and relative species abundance in ecology, *Nature* **424**, 1035 (2003).
- [22] M. Vallade and B. Houchmandzadeh, Analytical solution of a neutral model of biodiversity, *Physical Review E* **68**, 061902 (2003).
- [23] M. Loreau, N. Mouquet, and A. Gonzalez, Biodiversity as spatial insurance in heterogeneous landscapes, *Proceedings of the National Academy of Sciences* **100**, 12765 (2003).
- [24] J. Denk and O. Hallatschek, Self-consistent dispersal puts tight constraints on the spatiotemporal organization of species-rich metacommunities, *PNAS* **119**, 26 (2022).
- [25] G. Garcia Lorenzana, A. Altieri, and G. Biroli, Interactions and migration rescuing ecological diversity, *PRX Life* **2**, 013014 (2024).
- [26] R. Lande, S. Engen, and B.-E. Saether, *Stochastic population dynamics in ecology and conservation* (Oxford University Press, Apr. 2003).
- [27] S. Nee, The neutral theory of biodiversity: do the numbers add up?, *Functional Ecology* **19**, 173 (2005).
- [28] D. Kessler, S. Suweis, M. Formentin, and N. M. Shnerb, Neutral dynamics with environmental noise: age-size statistics and species lifetimes, *Physical Review E* **92**, 022722 (2015).
- [29] M. Kalyuzhny, R. Kadmon, and N. M. Shnerb, A neutral theory with environmental stochasticity explains static and dynamic properties of ecological communities, *Ecology Letters* **18**, 572 (2015).
- [30] M. Danino and N. M. Shnerb, Theory of time-averaged neutral dynamics with environmental stochasticity, *Physical Review E* **97**, 042406 (2018).
- [31] D. Gravel, C. D. Canham, M. Beaudet, and C. Messier, Reconciling niche and neutrality: the continuum hypothesis, *Ecology Letters* **9**, 399 (2006).
- [32] C. K. Fisher and P. Mehta, The transition between the niche and neutral regimes in ecology, *Proceedings of the National Academy of Sciences* **111**, 13111 (2014).
- [33] B. Haegeman and M. Loreau, A mathematical synthesis of niche and neutral theories in community ecology, *Journal of Theoretical Biology* **269**, 150 (2011).
- [34] G. Bunin, Ecological communities with Lotka-Volterra dynamics, *Phys. Rev. E* **95**, 042414 (2017).
- [35] M. Barbier, J.-F. Arnoldi, G. Bunin, and M. Loreau, Generic assembly patterns in complex ecological communities, *PNAS* **115**, 2156 (2018).
- [36] M. Advani, G. Bunin, and P. Mehta, Statistical physics of community ecology: a cavity solution to macarthur's consumer resource model, *Journal of Statistical Mechanics: Theory and Experiment* **2018**, 033406 (2018).
- [37] W. Cui, R. Marsland, and P. Mehta, Diverse communities behave like typical random ecosystems, *Physical Review E* **104**, 034416 (2021).
- [38] D. W. Purves and L. A. Turnbull, Different but equal: the implausible assumption at the heart of neutral theory, *Journal of Animal Ecology* **79**, 1215 (2010).
- [39] M. Barbier and J.-F. Arnoldi, The cavity method for community ecology, *bioRxiv*, 10 . 1101 / 147728 (2017).
- [40] F. Roy, M. Barbier, G. Biroli, and G. Bunin, Complex interactions can create persistent fluctuations in high-diversity ecosystems, *PLOS Comput. Biol.* **16**, e1007827 (2020).
- [41] M. T. Pearce, A. Agarwala, and D. S. Fisher, Stabilization of extensive fine-scale diversity by ecologically driven spatiotemporal chaos, *PNAS* **117**, 14572 (2020).
- [42] I. Dalmedigos and G. Bunin, Dynamical persistence in high-diversity resource-consumer communities, *PLOS Computational Biology* **16**, e1008189 (2020).
- [43] E. Mallmin, A. Traulsen, and S. De Monte, Chaotic turnover of rare and abundant species in a strongly interacting model community, *Proceedings of the National Academy of Sciences* **121**, 10 . 1073 / pnas . 2312822121 (2024).
- [44] E. Blumenthal, J. W. Rocks, and P. Mehta, Phase transition to chaos in complex ecosystems with nonreciprocal species-resource interactions, *Physical Review Letters* **132**, 127401 (2024).

- [45] T. Arnoulx de Pirey and G. Bunin, Many-species ecological fluctuations as a jump process from the brink of extinction, *Physical Review X* **14**, 011037 (2024).
- [46] O. Malcai, O. Biham, P. Richmond, and S. Solomon, Theoretical analysis and simulations of the generalized lotka-volterra model, *Physical Review E* **66**, 031102 (2002).
- [47] A. Melbinger and M. Vergassola, The impact of environmental fluctuations on evolutionary fitness functions, *Scientific Reports* **5**, 10.1038/srep15211 (2015).
- [48] E. H. van Nes, D. G. F. Pujoni, S. A. Shetty, G. Straatsma, W. M. de Vos, and M. Scheffer, A tiny fraction of all species forms most of nature: rarity as a sticky state, *Proceedings of the National Academy of Sciences* **121**, 10.1073/pnas.2221791120 (2024).
- [49] D. A. Kessler and N. M. Shnerb, Dominance to egalitarian transition in diverse communities, *arxiv*, 10.48550/arXiv.2407.08451 (2024).
- [50] A. M. Dean and N. M. Shnerb, Stochasticity-induced stabilization in ecology and evolution: a new synthesis, *Ecology* **101**, 10.1002/ecy.3098 (2020).
- [51] P. L. Chesson and R. R. Warner, Environmental variability promotes coexistence in lottery competitive systems, *The American Naturalist* **117**, 923 (1981).
- [52] E. C. Johnson and A. Hastings, Towards a heuristic understanding of the storage effect, *Ecology Letters* **25**, 2347 (2022).
- [53] J. Pande and N. M. Shnerb, How temporal environmental stochasticity affects species richness: destabilization, neutralization and the storage effect, *Journal of Theoretical Biology* **539**, 111053 (2022).
- [54] G. Pesce, A. McDaniel, S. Hottovy, J. Wehr, and G. Volpe, Stratonovich-to-itô transition in noisy systems with multiplicative feedback, *Nature Communications* **4**, 10.1038/ncomms3733 (2013).
- [55] J. Hofbauer and K. Sigmund, *Evolutionary games and population dynamics* (Cambridge University Press, 2002).
- [56] B. Derrida, Random-energy model: limit of a family of disordered models, *Physical Review Letters* **45**, 79 (1980).
- [57] P. Chesson and J. J. Kuang, The interaction between predation and competition, *Nature* **456**, 235 (2008).
- [58] G. Barabás, R. D’Andrea, and S. M. Stump, Chesson’s coexistence theory, *Ecological Monographs* **88**, 277 (2018).
- [59] R. H. MacArthur and E. O. Wilson, *The theory of island biogeography*, Vol. 1 (Princeton university press, 1967).
- [60] I. Eliazar, *Power laws: a statistical trek* (Springer International Publishing, 2020).
- [61] J. A. Fuhrman, J. A. Cram, and D. M. Needham, Marine microbial community dynamics and their ecological interpretation, *Nature Reviews Microbiology* **13**, 133 (2015).
- [62] G. Barabás, R. D’Andrea, R. Rael, G. Meszéna, and A. Ostling, Emergent neutrality or hidden niches?, *Oikos* **122**, 1565 (2013).
- [63] N. Leibovich, J. Rothschild, S. Goyal, and A. Zilman, Phenomenology and dynamics of competitive ecosystems beyond the niche-neutral regimes, *Proceedings of the National Academy of Sciences* **119**, 10.1073/pnas.2204394119 (2022).
- [64] J. Grilli, Macroecological laws describe variation and diversity in microbial communities, *Nat. Commun.* **11**, 4743 (2020).
- [65] L. Descheemaeker and S. de Buyl, Stochastic logistic models reproduce experimental time series of microbial communities, *eLife* **9**, e55650 (2020).
- [66] A. E. Magurran and P. A. Henderson, Explaining the excess of rare species in natural species abundance distributions, *Nature* **422**, 714 (2003).
- [67] G. Yenni, P. B. Adler, and S. K. M. Ernest, Do persistent rare species experience stronger negative frequency dependence than common species?, *Global Ecology and Biogeography* **26**, 513 (2017).
- [68] J. Rovere and J. W. Fox, Persistently rare species experience stronger negative frequency dependence than common species: a statistical attractor that is hard to avoid, *Global Ecology and Biogeography* **28**, 508 (2019).
- [69] R. May, Will a large complex system be stable?, *Nature* **238**, 413 (1972).
- [70] L. Buche, J. W. Spaak, J. Jarillo, and F. De Laender, Niche differences, not fitness differences, explain predicted coexistence across ecological groups, *Journal of Ecology* **110**, 2785 (2022).
- [71] B. W. Ji, R. U. Sheth, P. D. Dixit, K. Tchourine, and D. Vitkup, Macroecological dynamics of gut microbiota, *Nature Microbiology* **5**, 768 (2020).
- [72] L. Descheemaeker, J. Grilli, and S. de Buyl, Heavy-tailed abundance distributions from stochastic Lotka-Volterra models, *Physical Review E* **104**, 034404 (2021).
- [73] X.-W. Wang and Y.-Y. Liu, Origins of scaling laws in microbial dynamics, *Physical Review Research* **5**, 013004 (2023).
- [74] R. Maskawa, H. Takayasu, L. Takayasu, W. Suda, and M. Takayasu, Stochastic spatiotemporal growth model reproducing the universal statistical laws of the gut microbiome, *Physical Review Research* **7**, 013269 (2025).
- [75] D. T. Gillespie, Exact numerical simulation of the ornstein-uhlenbeck process and its integral, *Physical Review E* **54**, 2084 (1996).

- [76] B. Derrida, Random-energy model: an exactly solvable model of disordered systems, *Physical Review B* **24**, 2613 (1981).
- [77] P. Vivo, Large deviations of the maximum of independent and identically distributed random variables, *Eur. J. Phys.* **36**, 055037 (2015).

Supplementary Information
Fluctuating growth rates link turnover and unevenness in species-rich communities

Emil Mallmin^{1,*}, Arne Traulsen¹, and Silvia De Monte^{1,2}

¹Max Planck Institute for Evolutionary Biology, Plön, Germany

²Institut de Biologie de l'ENS (IBENS), Département de Biologie, Ecole Normale Supérieure,
CNRS, INSERM, Université PSL, 75005 Paris, France

*mallmin@evolbio.mpg.de

Wednesday 11th June, 2025

Supplementary Figures

S1	Sets of abundance distributions sharing rescaled intraspecific suppression and rescales immigration rates.	2
S2	Time-evolution of the SAD with or without coexistence mechanisms	3
S3	Turnover measured by Bray-Curtis decay corresponding to the panels in Figure S1.	4
S4	Turnover measured by Bray-Curtis decay corresponding to Main Text Figure 6.	4
S5	Distribution of mean abundances for the panels in Main Text Figure 6.	5

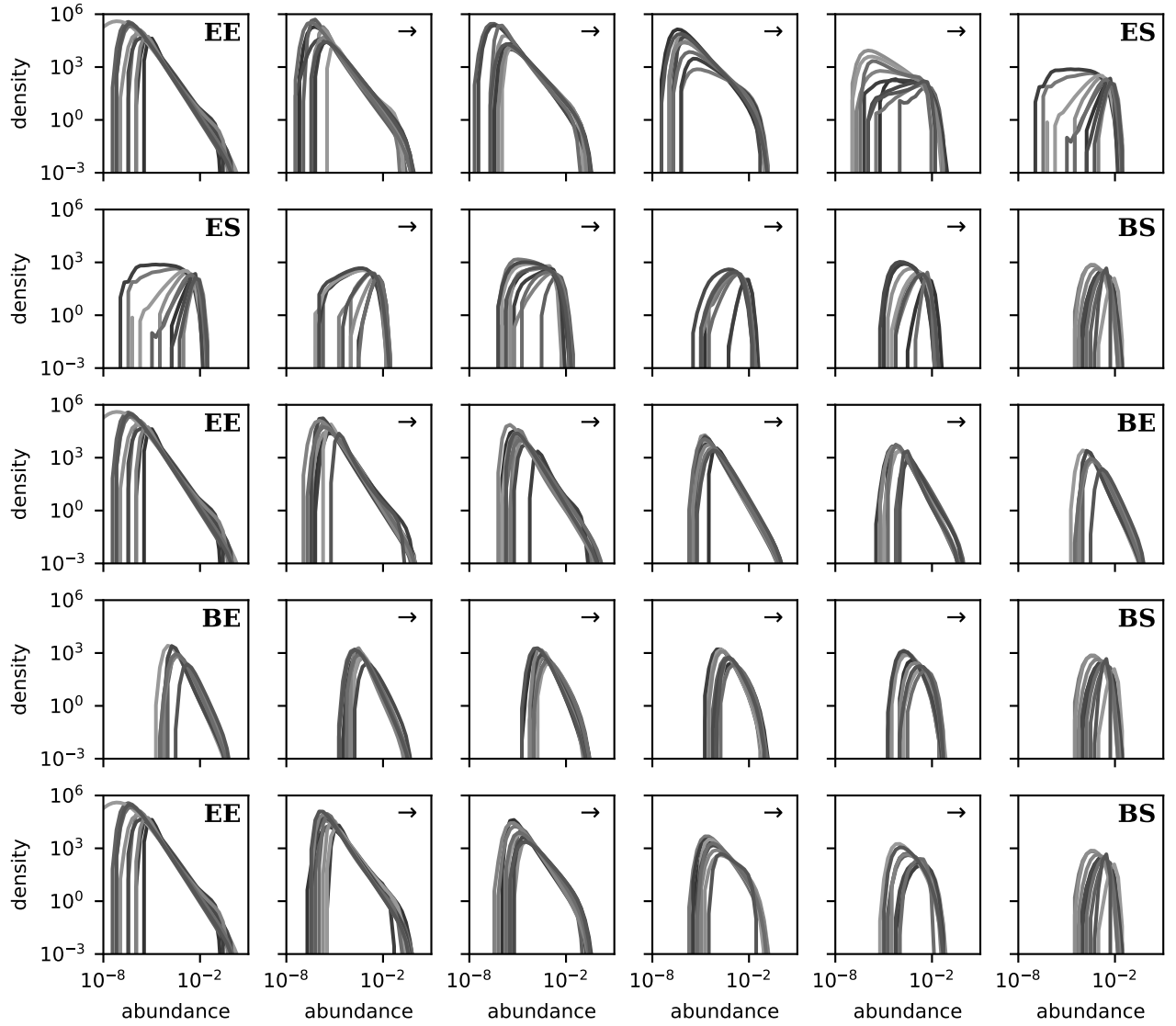


Figure S1: Sets of abundance distributions sharing rescaled intraspecific suppression and rescales immigration rates. (With reference to Main Text Figure 5.) Here we show the distribution sets that lie on a straight line between the reference cases, e.g. between EE and BS, in the upper row; EE and BE in the second row; and so on. The difference in line colors are just a guide for the eye.

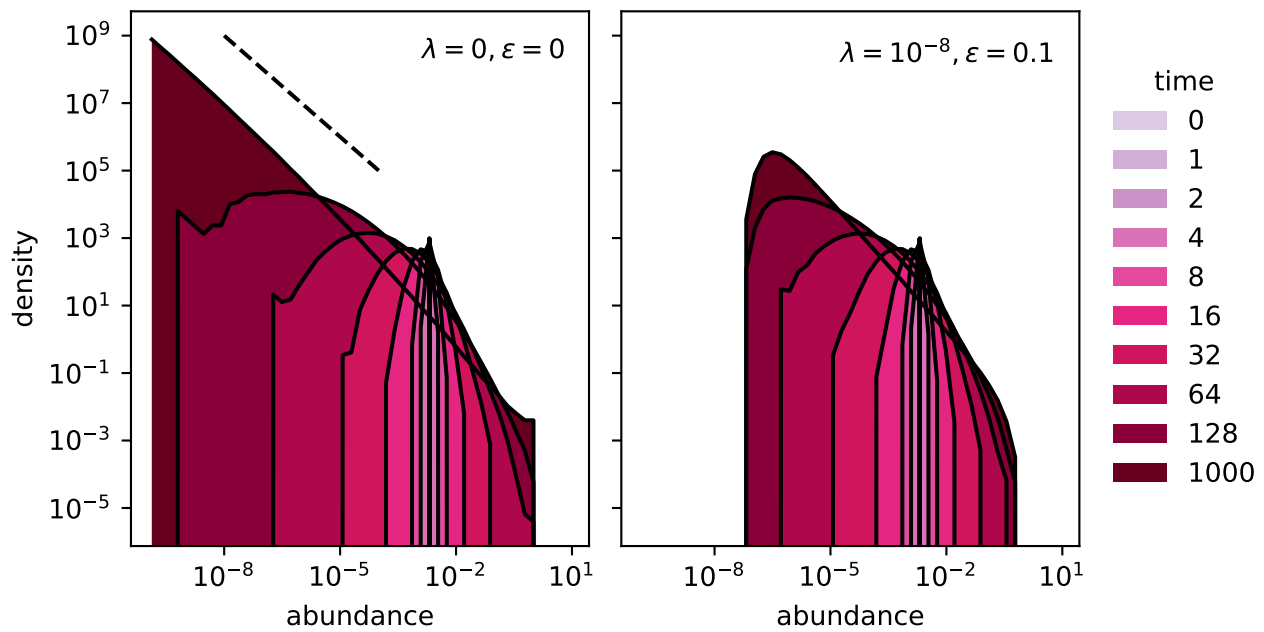


Figure S2: Time-evolution of the SAD with or without coexistence mechanisms. Starting from an even initial condition, we track the evolution of the SAD averaged over 1000 realizations. In the left panel, there is no immigration and no additional self-suppression, in contrast to the right panel. Early on, both scenarios give similar distributions, until the bounds in the latter scenario restrict the expansion of the distribution; for the former scenario, the power-law section extends ever into lower abundance decades with time, seemingly approaching an exponent of 1 (dashed line). Here, $S = 500, r^* = 1, \sigma_r = 0.05, \tau = 10$.

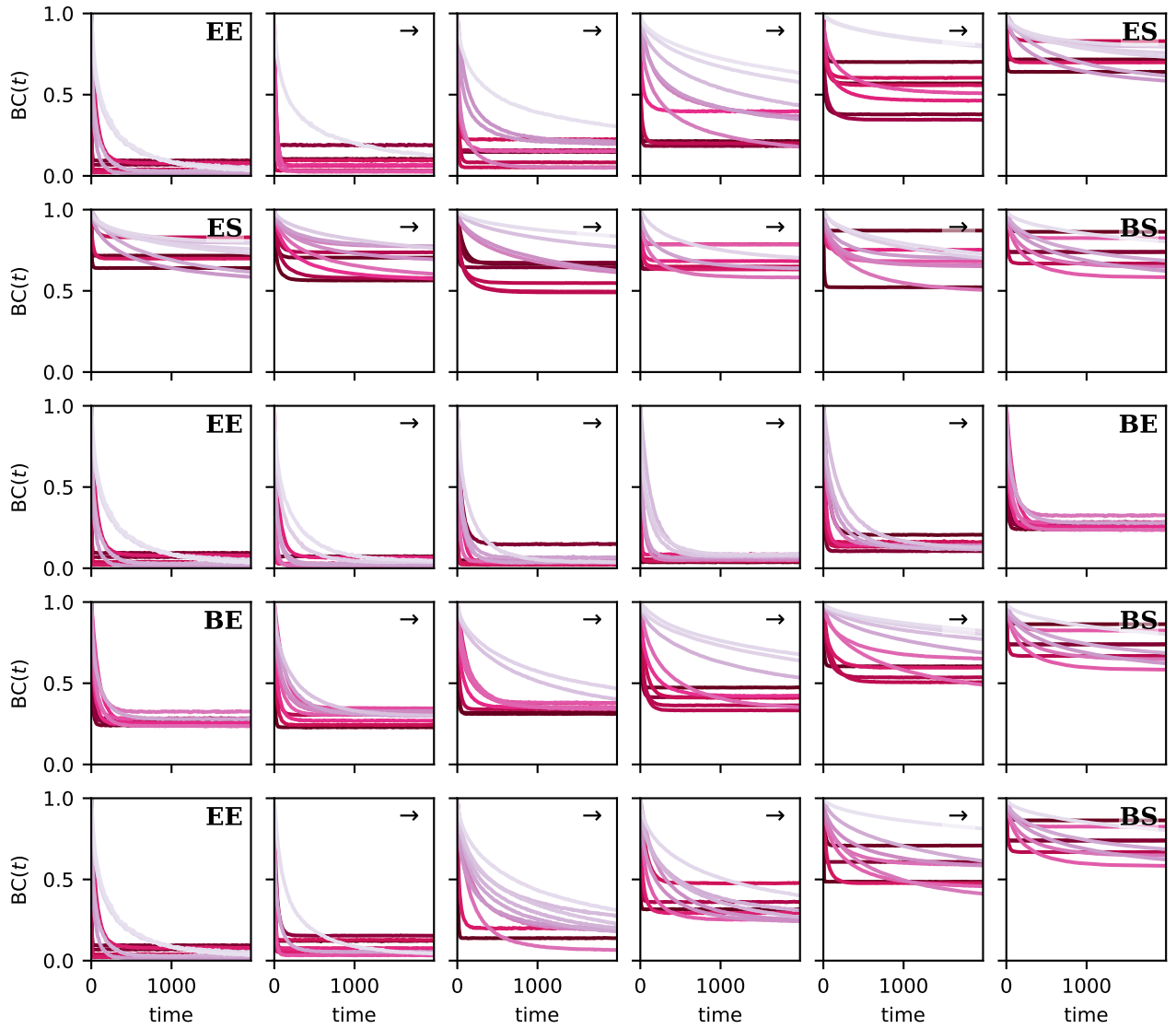


Figure S3: Turnover measured by Bray-Curtis decay corresponding to the panels in Figure S1. The color of the line reflects the value of $\log_{10} \gamma$, normalized separately for each panel. Light colors for small γ , dark color for large. Note that small γ gives slower decay, and that narrow SADs are associated with high limit of the BC.

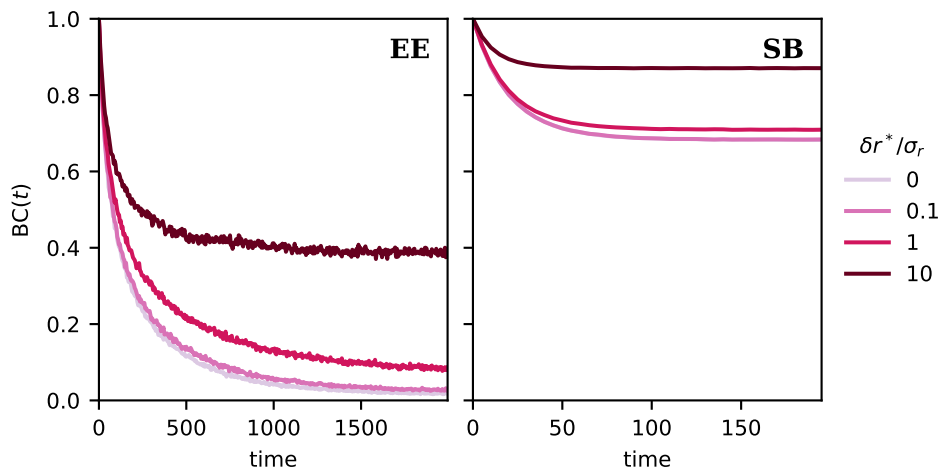


Figure S4: Turnover measured by Bray-Curtis decay corresponding to Main Text Figure 6. For each scenario (row) of Main Text Figure 6, each of the four panels with different $\delta r^* / \sigma_r$ corresponds to one line. Note the 10x difference in timescale between the two scenarios.

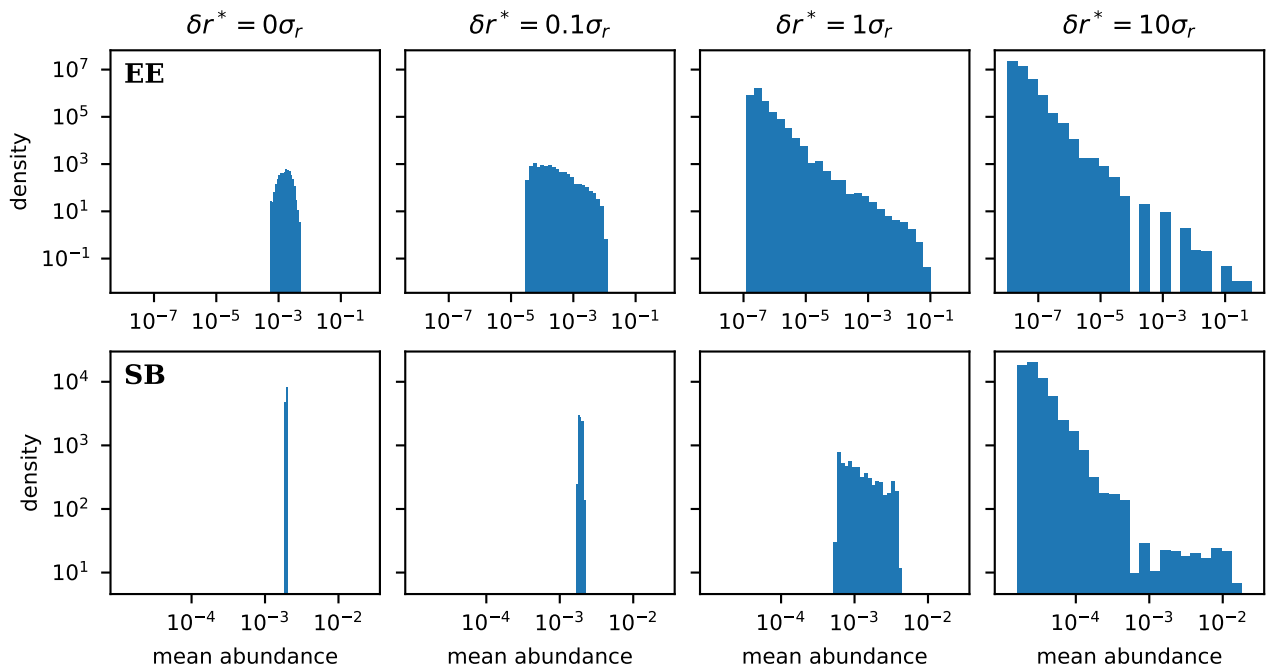


Figure S5: Distribution of mean abundances for the panels in Main Text Figure 6. Breaking time-averaged neutrality produces a distribution of species means. Note that the panels of the first column are TAN, so theoretically all species would have the same mean if the sampling time window was infinite. Note also the difference in scale of the horizontal axis of the two rows.